Experimental Neurology 332 (2020) 113389

Contents lists available at ScienceDirect

Experimental Neurology

journal homepage: www.elsevier.com/locate/yexnr

Research paper

MicroRNA-153 impairs hippocampal synaptic vesicle trafficking *via* downregulation of synapsin I in rats following chronic cerebral hypoperfusion

Shuai Zhang[1], Mei-Ling Yan[1], Lin Yang, Xiao-Bin An, Hong-Mei Zhao, Sheng-Nan Xia, Zhuo Jin, Si-Yu Huang, Yang Qu, Jing Ai*

Department of Pharmacology (The State-Province Key Laboratories of Biomedicine-Pharmaceutics of China), College of Pharmacy of Harbin Medical University, Harbin, Heilongjiang Province 150086, China

ARTICLE INFO

Keywords:
Chronic cerebral hypoperfusion
Synapsin
microRNA-153
Synaptic vesicle trafficking
Delayed response enhancement

ABSTRACT

Chronic cerebral hypoperfusion (CCH) promotes the development of Alzheimer's pathology. However, whether and how CCH impairs the synaptic vesicle trafficking is still unclear. In the present study, we found that the hippocampal glutamatergic vesicle trafficking was impaired as indicated by a significant shortened delayed response enhancement (DRE) phase in CA3-CA1 circuit and decreased synapsin I in CCH rats suffering from bilateral common carotid artery occlusion (2VO). Further study showed an upregulated *miR-153* in the hippocampus of 2VO rats. *In vitro,* overexpression of *miR-153* downregulated synapsin I by binding the 3′UTRs of *SYN1* mRNAs, which was prevented by its antisense AMO-153 and miRNA-masking antisense oligodeoxynucleotides (*SYN1-ODN*). *In vivo*, the upregulation of *miR-153* elicited similar reduced DRE phase and synapsin I deficiency as CCH. Furthermore, *miR-153* knockdown rescued the downregulated synapsin I and shortened DRE phase in 2VO rats. Our results demonstrate that CCH impairs hippocampal glutamatergic vesicle trafficking by upregulating *miR-153*, which suppresses the expression of synapsin I at the post-transcriptional level. These results will provide important references for drug research and treatment of vascular dementia.

1. Introduction

Similar to amyloid-beta (Aβ) plaques, Tau hyperphosphorylation, and cell death, synaptic pathology also plays a prominent role in the occurrence of Alzheimer's disease (AD) and vascular dementia (VaD) (Selkoe, 2002; Forner et al., 2017). Aberrant neurotransmitter release, elicited from either Aβ aggregation or not, is proposed to be a crucial early event and directly tied to disease severity (Rajmohan and Reddy, 2017; He et al., 2019). It has been known that chronic cerebral hypoperfusion (CCH) is a key predictor of the conversion from mild cognitive impairment (MCI) to AD or VaD (Pantoni, 2010; de la Torre, 2018). CCH was also found to promote the amyloidogenic processes and tau hyperphosphorylation (Ai et al., 2013; Liu et al., 2016), as well as synaptic plasticity deficiency (Chen et al., 2017; Bhuvanendran et al., 2019). However, whether CCH affects presynaptic plasticity by disturbing neurotransmitter release is still unknown.

Neurotransmitter is controlled by a battery of conserved protein machinery (Sudhof, 2013b; Hackett and Ueda, 2015), which disparts presynaptic neurotransmitter into three functional vesicle pools: the reserve pool making up ~80–90% of the total pool; the readily releasable pool (RRP) consisting of a few vesicles (~1%) that were docked and primed for transmitter releasing; and the recycling pool (~10–15%) that is thought to traffic neurotransmitter from reserve pool to RRP to maintain the highly efficiency of neurotransmitter release from RRP to synaptic cleft (Rizzoli and Betz, 2005). Vesicles trafficking from the reserve pool to the RRP are regulated by synapsin I/II and its co-factor CaMK II (Benfenati et al., 1992, Torri et al., 1992, Rizzoli and Betz, 2005), which was found for the release of glutamate in excitatory hippocampal synapses (Gitler et al., 2004; Bogen et al., 2009; Song and Augustine, 2015). The process of the synaptic vesicle trafficking can be visualized by an electrophysiological index-delayed response enhancement (DRE). Synapsins knockout mice displayed memory deficits and loss of DRE (Jensen et al., 2007; Corradi et al., 2008; Bogen et al., 2011), indicating the close relationship between DRE maintenance and cognition. Previous studies have already reported the downregulation of synapsins in AD patients (Ho et al., 2001; Yao et al., 2003) and acute

* Corresponding author.
E-mail address: azhrbmu@126.com (J. Ai).
[1] Shuai Zhang and Mei-Ling Yan contributed equally to this work.

https://doi.org/10.1016/j.expneurol.2020.113389
Received 11 February 2020; Received in revised form 2 May 2020
Available online 21 June 2020

brain ischemia (Bolay et al., 2002; Hua et al., 2019). Nevertheless, how vesicle trafficking and its regulatory protein changed during CCH pathology is unknown.

Previous studies have reported that microRNAs (miRNAs), like *miR-153*, *miR-34a*, *miR-135a*, and *miR-137*, could regulate vesicle fusion with presynaptic membrane by targeting various vesicle-related proteins, such as VAMP-2 (vesicle-associated membrane protein 2, also known as synaptobrevin-2), SNAP-25 (synaptosomal-associated protein 25) and syntaxin-1 (also known as HPC-1) (Hu et al., 2015; Siegert et al., 2015; Mathew et al., 2016; Mannironi et al., 2018). However, whether miRNAs regulate vesicle trafficking through regulating the expression of synapsins is unclear. Furthermore, plenty of studies have been demonstrated that CCH induced AD-like pathologies were regulated by various miRNAs (Ai et al., 2013; Sun et al., 2015; Che et al., 2017; Fang et al., 2017; Zhang et al., 2017), suggesting that miRNAs have the potential to regulate vesicle trafficking by binding with vesicle trafficking-related genes.

In the present study, we firstly reported that CCH impaired hippocampal glutamatergic synaptic vesicle trafficking, which was controlled by upregulated m*iR-153* mediated downregulation of synapsin I through binding the 3′UTR of synapsin I coding gene *SYN1*. Over-expression of *miR-153* in rat hippocampus could mimic the effects of CCH *in vivo*. The knockdown of *miR-153* may be a new strategy for alleviating the synaptic pathology of VaD.

2. Materials and methods

2.1. Animals

The total 60 male Sprague-Dawley (SD) rats (5–6 months old) and 6 male mice (5–6 months old) were obtained from the Animal Center of the Second Affiliated Hospital of Harbin Medical University (Harbin, Heilongjiang Province, China). All the animals for experiments were housed at 23 ± 1 °C with 55 ± 5% of humidity and maintained on 12 h dark-light artificial cycle (lights on at 7:00 A.M.) with food and water available *ad libium*. Samples for qRT-PCR and western blot assay were obtained from the rat hippocampus after they had been anesthetized with 10% chloral hydrate (500 mg/kg, intraperitoneal (Aladdin, Cat. No. C104202, Shanghai, China) followed by confirmation of death by exsanguination. Tissues for primary neuron culture were from neonatal SD rats after administration of 20% isoflurane and confirmation of death by cervical dislocation. All animal procedures were approved by the Institutional Animal Care and Use Committee at Harbin Medical University (No. HMUIRB-2008-06) and the Institute of Laboratory Animal Science of China (A5655–01). All procedures were conformed to the Directive 2010/63/EU of the European Parliament.

2.2. Permanent, bilateral common carotid artery occlusion (2VO) in the rat

The method for preparation of 2VO rat was described as previously (www.bio-protocol.org/e2668) (Ai et al., 2013). Briefly, 40 rats (26 for 2VO surgery, 14 for sham surgery) had access to water but not food for 12 h before surgery. After anesthetized with 10% chloral hydrate (300 mg/kg), rats were mounted to an electric heating pad (Dongxiyi, Cat. No. wi95919, Beijing, China) to maintain body temperature at 37 °C. Then the fur around neck was clean with an electric shaver and skin was sterilized with 75% alcohol cotton ball. Through a 1.5–2 cm midline cervical incision, both common carotid arteries were carefully exposed and doubly ligated with 3–0 silk suture (Jinhuan, model: 3–0, China). The sham-operated animals were treated similarly to the 2VO rats without common carotid artery ligations. To avoid potential post-operative infection, 20 mg/mL gentamycin sulfate solution (Sangon biotech, Cat. No. B540724) was used to wash the wound. The wounds were then sutured and rats were allowed to recover from anesthesia before being returned back to their cages. Three of the 26 2VO rats (11.5%) were dead due to the surgery. No rat was dead from sham surgery.

2.3. Construction of lentivirus vectors

Lenti-*pre-miR-153*, the *miR-153-3p* overexpression plasmid (RmiR6060-MR03, GeneCopoeia, Guangzhou, China) or negative control (NC) using scrambled RNA oligonucleotides of *miR-153* (Lenti-mis-pre-*miR-153-3p*) (CmiR0001-MR03, GeneCopoeia, Guangzhou, China) were generated with the pEZX-MR03 lentiviral transfer vector. While, the *miR-153* inhibitor plasmid Leni-AMO-*miR-153-3p* or negative control (NC) of *AMO-153* using scrambled RNA oligonucleotides (Leni-mis-AMO-*miR-153-3p*), were generated with pEZX-AM03 (RmiR-AN0214-AM03, GeneCopoeia, Guangzhou, China). The titers of these RNA oligonucleotides vectors used for experiments were 1×10^8 transducing U/mL. Virus suspensions were stored at −80 °C until use and were briefly centrifuged and kept on ice immediately before injection.

2.4. Stereotaxic injection of the lentiviral vectors

After 1-month of normal feeding or sham/2VO surgery, rats were anesthetized and head-fixed to a stereotaxic frame (RWB Life Science Co. Ltd., China). Two μL (10^5 TU/μL) Lenti-*pre-miR-153-3p,* Lenti-AMO-*miR-153-3p,* Lenti-mis-pre-*miR-153-3p* and/or Leni-mis-AMO-*miR-153-3p* was injected into bilateral CA1 regions of the hippocampus using a 5 μL Hamilton syringe with a 33-gauge tip needle (Hamilton, Bonaduz, Switzerland) at a rate of 0.5 μL/min. Injection coordinates relative to the bregma were anteroposterior −3.60 mm; mediolateral ± 2.30 mm; dorsoventral −3.00 mm using coordinates derived from the atlas of Paxinos and Watson. The needle was left in place for 5 mins before retraction. Once the needle was retracted, the incision was closed with a silk suture (Ai et al., 2013).

2.5. Electrophysiology

Acute hippocampal slice preparation (Mathis et al., 2011). After 2-month of sham/2VO surgery or 1-month of intra-hippocampal injection of the lentiviral vectors, the rats were anesthetized with 20% urethane intraperitoneally and decapitated. The wound was immediately placed on ice-cold dissection buffer for 10 s (NMDG solution in mM: 93 NMDG, 2.5 KCl, 10 $MgSO_4$, 1.2 NaH_2PO_4, 30 $NaHCO_3$, 20 HEPES, 0.5 $CaCl_2$, 25 D-glucose, 5 Sodium-ascorbate, 3 Sodium-Pyruvate, 2 thiourea and 2 N-Acetyl-L-cystein, with pH 7.3–7.4 adjusted by NaOH or HCl and saturated with O_2 (95%)/CO_2 (5%) carbogen mixture). Next, the brain hemispheres were put in the ice-cold NMDG solution for 60 s after carefully removing the skull. Using a Leica VT1200S microtome (Leica, Nussloch, Germany), transverse hippocampal slices (400 μm thick) were prepared with 0.8 mm cut amplitude and 0.4 mm/s advance speed. The slices were then transferred into 28 °C NMDG solution for a 3-min recovery, and sequentially maintained in an O_2 (95%)/CO_2 (5%)-saturated incubation solution containing (in mM): 124 NaCl, 2.5 KCl,1.2 NaH_2PO_4, 24 $NaHCO_3$, 2 $MgSO_4$, 2 $CaCl_2$, 5 HEPES, 2 N-Acetyl-L-cystein, and 12.5 D-glucose (pH 7.3–7.4) for at least 1 h at 33 ± 2 °C. Individual slice was transferred to recording chamber and repose at least 15 min before recording. The slices were maintained in standard artificial cerebrospinal fluid (ACSF) solution at a constant flow (2–3 mL/min), ACSF solution (in mM): 124 NaCl, 2.5 KCl, 1.2 NaH_2PO_4, 24 $NaHCO_3$, 2 $CaCl_2$, 2 $MgSO_4$, 5 HEPES and 10 D-glucose. Slices for experiments of frequency stimuli were placed in a humidified interface chamber where the temperature was kept constant at 24 °C or 29 °C with bath application of 50 μmol/L 2-amino-5-phosphopentanoic acid (AP5, Abcam) to avoid NMDA receptor-mediated synaptic plasticity. Picrotoxin (50 μmol/L) was used to block the function of GABA.

Extracellular Recordings. A concentric bipolar microelectrodes (CBARC75, FHC, USA) was placed in the schaffer collateral (SC) domain with a 300 μm distance away from recording pipettes. Extracellular recordings were made in the stratum radiatum of CA1 area using

recording pipettes pulled from borosilicate glass (BF100–58-10, Sutter Instrument) with resistances of 2–3 MΩ when filled with a NaCl (3 mol/L) solution. Field excitatory postsynaptic potentials (fEPSPs) of SC-CA1 were evoked by current stimuli with stimulatory isolator (ISO-Flex (AMPI, Jerusalem,Israel) controlled by Master-8 pulse generator (AMPI, Jerusalem, Israel). The stimulus intensities which corresponds to the ~50% of maximum amplitude of fEPSPs was used for synaptic plasticity evaluation. Analogue signals were bypass filtered and digitized at 6 kHz using a Digidata 1550A and pClamp10 software (Molecular Devices, US). Timing dependent facilitation and depression in SC-CA1 synapses were recorded using the frequencies of 10 Hz and 20 Hz after stable synaptic responses (0.033 Hz stimulation) for at least 10–15 min (Jensen et al., 2007; Hvalby et al., 2010; Bogen et al., 2011).

Signal analysis Off-line analysis was performed using Clampfit software (Molecular Devices, US). According to previous reports, frequency dependent synaptic response evaluation was divided into three distinct time points which were ranked to characterize the time courses following increased stimulus number, *i.e.* "*a*" represents the time needed to arrive the maximal magnitude of the initial frequency facilitation; "*b*" stands the inflection point between the first fast decay response and the beginning of a relative gentle decline; and "*c*" is the inflection point between the relative gentle decline and subsequent fast decay. The period between the point "*b*" and "*c*" is defined as delayed response enhancement (DRE) (Jensen et al., 2007; Hvalby et al., 2010; Bogen et al., 2011).

2.6. Dual luciferase reporter assay

Plasmid construction The design of plasmid was shown as Fig. 3b. Full length 3′UTR and mutant 3′UTR of *SYN1* genes containing the putative binding sequences for *miR-153* were amplified by PCR: The sequences were following:

SYN1–3′UTR: (the binding site of *miR-153* is marked by bold italic characters).

ccaggatgaggtgaaagctga-
gaccatccgcagcctgaggaagtctttcgccagcctcttctccgactgacaccctactctga-
gaaccctaaacccctaga-
caaccctctctgggtcctgagtccatttctcacctttggaatctccaaatcccttga-
gaaccctctctctcctggttctacatcccacttctcattcctcaagatgtcccttga-
gaaacgtggtcctaaatccagttctcacattgggaatccccaagtccattta-
gaatcctgttcccagtcacctccagatctgttttagaatctccaaattcctgaagacctctacttctga-
tatctctaaagggtgatttcctccctggaagttcctgaatggcagaacctgtttctgacctaata-
catcctctcctggagctctggaattcctggaaaaccctattctactcttggtcctgaatctctccagca-
caccttgctcctaatcagaagtttcaaattccaaaagaagcccctatccttaaatctcttccta-
gattatctctctgga-
gagccacctcttcaaatgccacctactatccaccaaccagtccctcaaggacttcctttc-
cacctcttccctcaaccccattcaaca-
tactggaagttccttccacttctaggacccctaagttccttcctcca-
gaaacctcctccccaatctcctgcctctgacagctgtctttaaa***tatgcaa***actctacccatcctctca-
gaatcctttgca-
caagggaggcctaaggtctcccaccactcccccacctttgccaatgtttgtgtctgtgact-
gacttggcctccttttgtgccatgctaggcatatgtggtcctcattcgtgctgcctgtggtaatgtgta-
cagtggcgctgtttgtgtggtccgcatcttcctccaacctccactccttgcctggacttgccc-
caccctcagtggctctgaaccccaagagaagagtcgggaagcaaaataaa-
caagcaaaggcccagcagaa.

mutSYN1–3′UTR: (the mutated DNA sequences of *miR-153* binding site is marked by bold italic characters).

ccaggatgaggtgaaagctga-
gaccatccgcagcctgaggaagtctttcgccagcctcttctccgactgacaccctactctga-
gaaccctaaacccctaga-
caaccctctctgggtcctgagtccatttctcacctttggaatctccaaatcccttga-
gaaccctctctctcctggttctacatcccacttctcattcctcaagatgtcccttga-
gaaacgtggtcctaaatccagttctcacattgggaatccccaagtccattta-
gaatcctgttcccagtcacctccagatctgttttagaatctccaaattcctgaagacctctacttctga-
tatctctaaagggtgatttcctccctggaagttcctgaatggcagaacctgtttctgacctaata-
catcctctcctggagctctggaattcctggaaaaccctattctactcttggtcctgaatctctccagca-
caccttgctcctaatcagaagtttcaaattccaaaagaagcccctatccttaaatctcttccta-
gattatctctctgga-
gagccacctcttcaaatgccacctactatccaccaaccagtccctcaaggacttcctttc-
cacctcttccctcaaccccattcaaca-
tactggaagttccttccacttctaggacccctaagttccttcctcca-
gaaacctcctccccaatctcctgcctctgacagctgtctttaaa***atacgtt***actctacccatcctctca-
gaatcctttgca-
caagggaggcctaaggtctcccaccactcccccacctttgccaatgtttgtgtctgtgact-
gacttggcctccttttgtgccatgctaggcatatgtggtcctcattcgtgctgcctgtggtaatgtgta-
cagtggcgctgtttgtgtggtccgcatcttcctccaacctccactccttgcctggacttgccc-
caccctcagtggctctgaaccccaagagaagagtcgggaagcaaaataaa-
caagcaaaggcccagcagaa.

Genome templates were firstly extracted from rat tails with Wizard® genome DNA purification kit (Promega, Cat. No. A1125), and DNA electrophoresis was used to verify the quality of extracted genome. Then, PCR was employed to amplify the extracted genome, and PCR products were recollected with DNA Gel extraction kit (Dongsheng Biotech). Next, the recollected PCR products and psiCHECK-2 vectors were incubated with *XhoI* and *NotI* enzyme for enzymatic digestion. And enzyme digestive products were also recollected with DNA Gel extraction kit (Dongsheng Biotech). Finally, T4 DNA Ligase (TaKaRa, Cat. No. D2011A) was used to connect the target sequences and psiCHECK-2 vectors. The ligated products were then added into DH5α competent tissue for transformation. After cloning and enzymatic digestion of transformated plasmids, agarose gel electrophoresis and Blast analysis of cloned DNA sequencing relative to genes 3UTR published on NCBI were employed to verify the vector construction.

Mutagenesis nucleotides were carried out using direct oligomer synthesis for the 3′UTR region of *SYN1*. Point mutations were introduced into a possible *miR-153* binding site located in the 3′UTR region (Fig. 3a). The method of plasmid construction for carrying mutagenesis 3′UTRs was same as wild type plasmid construction.

Detection of dual Luciferase activities HEK293T cells (plated at 40% ~ 50% confluence) were transfected with 20 μmol/L *miR-153 mimic*, AMO-*miR-153*, or mis-*miR-153 mimic* siRNAs as well as 0.5 μg psi-CHECK™-2-target DNA (firefly luciferase vector) and 1 μL blank plasmid using lipofectamine 2000 (Invitrogen, USA) transfection reagent according to the manufacturer's instructions. Following transfection (48 h), luciferase activities were measured with a dual luciferase reporter assay kit (Cat. No. E1910, Promega, USA) on a luminometer (GloMax™ 20/20, Promega, USA); Nucleotide-substitution mutagenesis was carried out using direct oligomer synthesis for the 3′ UTRs of *SYN1*. All constructs were sequence verified.

2.7. Synthesis of miR-153, AMO-153 and other various oligonucleotides

The *miR-153* mimics (sense: 5′-UUGCAUAGUCACAAAAGUGAUC-3′; antisense: 5′-UCACUUUUGUGACUAUGCAAUU-3′), AMO-*miR-153* (5′-GAUCACUUUUGUGACUAUGCAA-3′), a scrambled *miR-153* RNA (mis-*miR-153*) used as a negative control of *miR-153* (sense: 5′-UUCU CCGAACGUGCACGUTT-3′; antisense: 5′-ACGUGACACGUUCGGAGA ATT-3′) and a scrambled AMO-153 RNA (mis-AMO-153) (5′-CAGUAC UUUUGUGUAGUACAA-3′) used as a negative control of AMO-153 were synthesized by Shanghai GenePharma Co, Ltd. (Shanghai, China). The synaptic proteins masking antisense oligodeoxynucleotides (ODNs) were synthesized by Shanghai Sangon Biological Engineering Technology and Service Co, Ltd. (Shanghai, China). *SNY1-ODN-1* was 5′-GGTAGAGTTTGCATATTTAAAG-3′, which complements in the position of 719–741 containing the binding sites of *miR-153* located in the position 727–733 of *SYN1* 3′ UTR. All nucleotides or deoxynucleotides at both ends of the antisense molecules were locked by a methylene bridge connecting between the 2′-O- and the 4′-C atoms.

2.8. Primary hippocampal and cortical neuron culture

Rat pups from the postnatal day 1–3 (P_{1-3}) were first anesthetized with isoflurane and decapitated, then the hippocampus and cortex were removed and put into cold phosphate buffer solution (PBS, Solarbio, Cat. No. P1010, Beijing). After dissected and triturated, tissues were digested in 0.25% trypsin digestive solution (Beyotime, Cat. No. C0201, Shanghai, China) for 15 min. Single cells were blew off after terminating digestion using culture media containing DMEM (Hyclone, Cat. No. SH30022.01, Logan, UT, USA) with 10% fetal bovine serum (FBS, HyClone, SH30070.02, Logan, UT, USA) and 1% penicillin-streptomycin (Beyotime, Cat. No. C0222, Shanghai, China), then they were plated on cell plates precoated with 10 μg/mL poly-D-lysine (PDL, Sigma, Cat. No. P0899, Saint Louis, CA, USA) and cultured in culture media containing neurobasal medium (Invitrogen, Cat. No. 21103049, Carlsbad, USA) with 2% B27 supplement (Invitrogen, Cat. No. 17504004, Carlsbad, CA, USA) without FBS. After 3 days, the neurons were treated with 5 μM cytosine arabinoside (Sigma, Cat. No. C8768, USA) to inhibit astrocyte proliferation. For the western blot and qRT-PCR experiments, the neurons were used six days after plating. Half volume of culture media was changed every three days (Ai et al., 2013).

2.9. Transfection procedures

Neonatal hippocampal and cortical neurons were transfected with 75 pmoL/mL *miR-153* mimics and/or AMO-153, ODNs, or mis-*miR-153* with X-treme GENE siRNA transfection reagent (Cat. No. 04476093001, Roche, USA), according to the manufacturer's instructions. Forty-eight hours after transfection, cells were collected for subsequent total RNA isolation or protein purification (Ai et al., 2013).

2.10. Quantitative real-time PCR

Total RNA samples were isolated with the trizol reagent (Invitrogen, Carlsbad, CA, USA), according to the manufacturer's instructions. *MiR-153* level was quantified by the ReverTra Ace® qPCR RT Kit (Code: FSQ-101, Osaka, Japan) and FastStart Universal SYBR® Green Master (Roche Diagnostics GmbH, Mannheim, Germany). The qRT–PCR probes and primers for *miR-153*, *U6* were designed by Invitrogen (Invitrogen, Carlsbad, CA, USA). QRT-PCR was performed on a LightCycle® 96 Instrument (Roche Diagnostics GmbH, Mannheim, Germany) for 40 cycles. Fold variations in miRNA expression between RNA samples were calculated after normalizing to the internal control, *U6*. (Ai et al., 2013).

2.11. Extraction of synaptosomes

The rats were sacrificed under 10% chloral hydrate anesthesia (300 mg/kg) and the blood was drained by intracardiac perfusion with chilled normal saline. The hippocampus was removed quickly and homogenized in 10% (*w/v*) of 320 mM sucrose HEPES buffer containing (in mM): 145 NaCl, 5 KCl, 2 $CaCl_2$, 1 $MgCl_2$, 5 glucose , 5 HEPEs with pH 7.3–7.4. Further, homogenate was centrifuged at 4–8 °C for 10 min at 600 ×g. The supernatant was then diluted 1:1 with 1300 mM sucrose HEPES buffer, to yield a suspension at a final concentration of 800 mM sucrose, and centrifuged at 4–8 °C for 15 min at 12000 ×g. The supernatant was discarded. The pellet consisting of synaptosomes was washed twice by HEPES buffer 12,000 ×*g* for 15 min at 4–8 °C to wash out the impurities. (Kamat et al., 2014).

2.12. Western blotting

Total protein samples were extracted from the rat hippocampal and cortical synaptosomes or primary cultured neurons. The protein content was determined by BCA Protein Assay Kit using bovine serum albumin as an internal standard. Protein samples fractionated on a 10% sodium dodecyl sulfate polyacrylamide gel electrophoresis gel were transferred to an NC membrane. Anti-synapsin 1 antibody (Cat. No. 106001; 1:1000; Synaptic Systems), anti-synapsin II antibody (Cat. No. 106211; 1:1000; Synaptic Systems), anti-CAMK II antibody (Cat. No. 13730–1-AP; 1:1000; Proteintech), and anti-P-syn I (Ser 603) antibody (Cat. No. PA1–4604; 1:1000; Rockford) were used. The day after incubation with the primary antibody, the membrane was incubated with secondary antibody diluted in PBS for 2 h at room temperature. Finally, western blot bands were captured using the Odyssey Infrared Imaging System (LI-COR Biosciences, Lincoln, NE, USA) and quantified using the Odyssey version 3.0 software by measuring the band intensity (area - OD). β-actin (Cat. No. 1:1000, G8795, Sigma) was used as an internal control for protein input.

2.13. Statistical analysis

Group data are expressed as mean ± SEM. All statistical analysis was performed in SPSS software (version 11). Each data set was analyzed for its ability to meet the statistical assumptions for equality of the variance, for normal distribution and for sphericity. Independent sample test was calculated using the Levene variance equality test. If $P > .05$, independent student's *t*-test was used for the comparison between two groups, If $P < .05$ Kruskal-Wallis rank sum test was performed. One Way ANOVA was performed for the comparison among multivariate groups and *Post hoc* analyses of significant main effect ware further examined using Fisher's PLSD tests.

3. Results

3.1. CCH impairs hippocampal synaptic vesicle trafficking in rats

Since no previous study described the DRE properties in rats, we firstly repeated the stimulating parameter in mouse model as the reference standard (Jensen et al., 2007; Bogen et al., 2011). We prepared hippocampal brain slices and monitored DRE properties by recording the field excitatory postsynaptic potentials (fEPSPs) in CA3-CA1 pathway (Fig. S1A). As illustrated in Fig. S1B, mouse hippocampal DRE was recorded following a prolonged stimulation at 10 and 20 Hz in SC-CA1 synapses at 29 °C, but it was absent in 24 °C. However, in rat hippocampus, 10 Hz but not 20 Hz stimulation elicited DRE at 29 °C. As shown in Fig. S1C, following 10 Hz stimulation, the transient frequency-dependent facilitation firstly reached a peak value at *a* seconds (~1 s), followed by a short-term steep decay to *b* seconds that reached an apparent reflection point (duration of 2–3 s). With further stimulation, frequency-dependent facilitation reached the DRE phase (between *b* and *c* seconds), a gentle decline phase maintained for approximately ~10 s (50–150 stimuli). After the DRE phase, fEPSP decay to 20% of the initial slope with fast speed. However, 20 Hz stimulation on rat SC-CA1 pathway only induces a sequential decline of fEPSP. Therefore, 10 Hz stimulation with 29 °C bath temperature was employed to evaluate the synaptic vesicle trafficking in our following experiments.

As previously described, bilateral common carotid artery ligation (2VO) surgery was performed to establish the CCH rat models (Farkas et al., 2007; Ai et al., 2013). After 8 weeks of 2VO surgery, we monitored the fEPSPs in hippocampal SC-CA1 pathway, and observed a significantly enhanced normalized fEPSP slope and shortened DRE phase compared with sham group (Fig. 1A & B). The trafficking of synaptic vesicles from the reserve pool to RRP was achieved by the activation of Ca^{2+}-dependent kinases, such as CaMK II that phosphorylate synapsin (Benfenati et al., 1992), and DRE was found to be abolished in mice devoid of synapsin I and II proteins using double knock-out mice (DKO) (Bogen et al., 2011). Therefore, we evaluated the expression level of synapsins, phospho-synapsins and CAMK II in rat hippocampus. We found that both the phosphorylated synapsin I levels and the protein expression levels of synapsin I and synapsin II were significantly decreased in the hippocampus of the 2VO rats. While the protein level

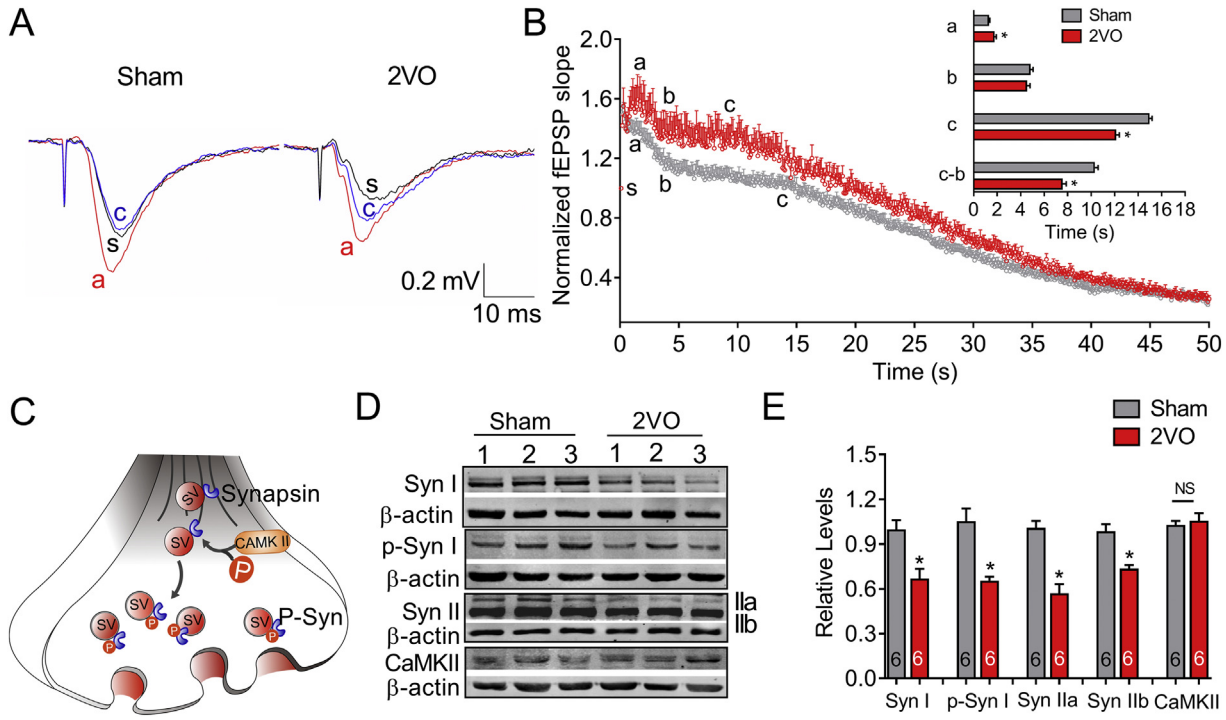

Fig. 1. CCH impairs hippocampal synaptic vesicle trafficking in rats. (A) Sample hippocampal fEPSP traces of sham and 2VO rats under 10 Hz electric stimulation. s trace (black), a trace (red), and c trace (blue) reflect the fEPSP at baseline, peak and DRE transition point during 10 Hz stimulation. (B) The average traces following 10 Hz frequency stimulation with the increase of recording time in rats SC-CA1 pathway. DRE duration decreased in the hippocampal SC of 2VO rats explored by afferent stimulation frequency of 10 Hz for 50 s (500 stimuli) performed at 29 ˚C. The insert shows a comparison of the changes of points *a*, *b*, *c*, and *c-b* (the duration of DRE) between Sham (gray, $n = 11$) and 2VO (red, $n = 8$) rats. $^*P < .05$ *vs* sham. (C) Schematic diagram showing molecular mechanism of presynaptic synapsin function. Synapsins (blue) binds to synaptic vesicles (SVs) and keeps the SVs in the reserve pool by tethering to the F-actin (gray) in the cytoskeleton. Whereas, CaMK II phosphorylated synapsins dissociate from F-actin. Meanwhile, the SVs trafficking to active zoom function as the docked SVs in the RRP. (D) Samples of western blot bands of synapsin I (Syn I), phosphorylated synapsin I (p-Syn I). synapsin IIa (Syn IIa), synapsin IIb (Syn IIb), and CAMK II. (E) Statistical analysis of synapsins and CaMK II protein expression. $^*P < .05$ *vs* sham, error bars, s. e. m. $n = 6$. (For interpretation of the references to colour in this figure legend, the reader is referred to the web version of this article.)

of CaMK II was not changed, suggesting that the decreased phosphorylation of synapsin I was not the result of CaMK II in 2VO rats (Fig. 1D & E). These results demonstrated that CCH downregulates the expression of synapsins and impairs the synaptic vesicle trafficking of SC-CA1 in rats.

3.2. MiR-153 targets synaptic vesicle protein synapsin I

Computational analysis with miRNA databases Targetscan revealed a conserved *miR-153* binding site at the position 727–733 bp on the 3′UTR of the *SYN1* gene (encoding synapsin I) (Fig. 2A). We speculated that *miR-153* might be involved in the downregulation of synapsin I. Using qTR-PCR technique, *miR-153* was found significantly upregulated (> 2 folds) in 2VO rats compared with sham rats (Fig. 2B). Next, to experimentally verify that synapsin I was the target of *miR-153*, we performed three experiments. First, we cloned the full length of the 3′UTRs of *SYN1* containing the *miR-153* binding sites into the luciferase-expressing reporter plasmid and then assessed the effects of *miR-153* on reporter activities in HEK293T cells (Fig. 2C). We found that the luciferase activity was significantly reduced when transfection of the psiCHECK™-2 vector plasmid containing chemically modified *miR-153* mimics compared with the transfection of the empty psiCHECK™-2 vector plasmid (blank) alone and psiCHECK™-2 vector plasmid containing oligoribonucleotides of either mis-*miR-153* or mis-AMO-153 in HEK-293 T cells (Fig. 2D). Mutations in the *SYN1* (727-733 bp) binding sites abolished the repressive effects of *miR-153* on the luciferase activities (Fig. 2E). Second, we designed the antisense AMO-153 as the antagonist of *miR-153* (Fig. 3A), and transfected *miR-153* mimic and its antisense AMO-153 using X-treme GENE siRNA transfection reagent into cultured neonatal rat neurons (NRNs). The successful transfection of *miR-153* and AMO-153 into NRNs was verified by qRT-PCR (Fig. 3B). As shown in Fig. 3C, we observed that *miR-153* effectively inhibited the expression of synapsin I relative to control group, whereas the scrambled *mis-miR-153* failed to affect the protein levels. In contrast, AMO-153 rescued the decreased expression of synapsin I inhibited by *miR-153*, indicating the sequence specificity of *miR-153* actions. Since the relationship between a miRNA and its targets is very complicated, the application of AMO-153 cannot exclude other relationships between *miR-153* and its targets. To verify the specific regulating effect of *miR-153* on synapsin I, we further designed an antisense oligodeoxynucleotide fragment, *SYN1-ODN*, which could specifically mask *miR-153* binding site on the 3′UTR of *SYN1* mRNA but retained the functions of *miR-153* on other targets (Fig. 3A). In this case, we found that masking the binding site of *miR-153* on the 3′UTR of *SYN1* gene at the position of 727-733 bp using the antisense oligodeoxynucleotide fragment of *miR-153* (*SYN1-ODN*) effectively blocked the repressive effects of *miR-153* on synapsin I (Fig. 3D). Therefore, the regulating effect of *miR-153* on the synapsin I is directly targeting the 3′UTR of SYN1 gene at the site of 727-733 bp.

3.3. MiR-153 impairs hippocampal synaptic vesicle trafficking

Subsequently, we investigated whether the upregulation of *miR-153* could affect synaptic vesicle trafficking *in vivo*. To test this notation, we designed the following three constructs in lentiviral vectors: scramble negative control lenti-pre-mis-*miR-153*, lenti-pre-*miR-153*, and lenti-AMO-153. These constructs were then injected directly into the bilateral hippocampal CA1 subfields of each rat according to a previous

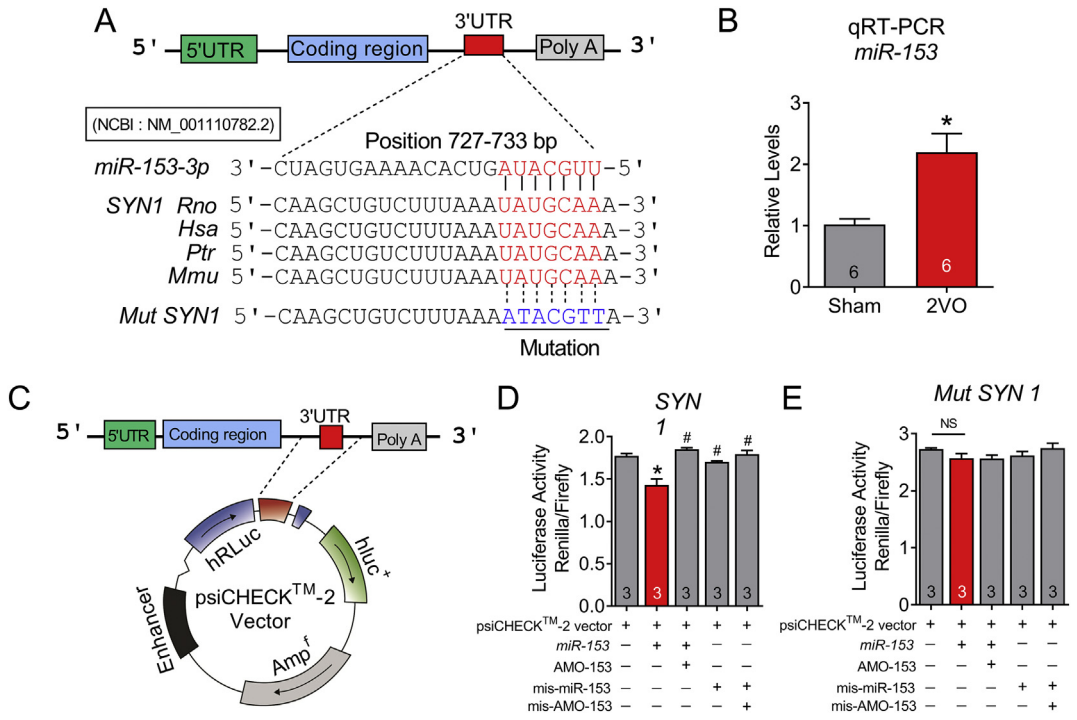

Fig. 2. *MiR-153* targets the 3′UTRs of SYN1 gene. (A) Conserved binding site of *miR-153* seed sequence (5′ end 7–8 nt) complementary with the 3′ UTR of rat's *SYN1* among rat, human, *Pan troglodytes* and mice, which were predicted by a computational and bioinformatics-based approach using the Targetscan 5.1 algorithm. (B) The levels of *miR-153* in the hippocampus of sham and 2VO rats as assessed by qRT-PCR. $^{*}P < .05$ *versus* Sham, n = 6. (C) Schematic diagram of plasmid construction for the luciferase assay. (D) Dual luciferase assay for interactions between *miR-153* and predicted binding sites in the 3′UTR of *SYN1* mRNA in HEK293T cells. (E) Dual luciferase assay for interactions between *miR-153* and mutant binding sites in the 3′UTR of *SYN1* mRNA in HEK293T cells. $^{*}P < .05$ *vs* psiCHECK™-2 vector, $^{\#}P < .05$ *vs miR-195*. Error bars, s. e. m.

protocol (Ai et al., 2013) (Fig. 4A). As illustrated in Fig. 4B, compared to the injection of lenti-pre-mis-*miR-153* oligonucleotide, the application of lenti-pre-*miR-153* produced a significantly high expression of *miR-153* (> 3-fold) in the rat hippocampus, which could be blocked by co-injection with lenti-AMO-153. As expected, we observed that the upregulation of *miR-153* by injecting lenti-pre-*miR-153* significantly inhibited synapsin I protein expression in the hippocampus (Fig. 4C) of the rats, and these effects were reversed by lenti-AMO-153 supplementation. We next evaluated the effects of *miR-153* on DRE maintenance. We observed that injection of lenti-pre-*miR-153* into the hippocampus of normal rats elicited significantly enhanced normalized fEPSP slope and shortened DRE duration (Fig. 4D & E), which prevented by the co-injection of lenti-AMO-153 (Fig. 4D & E). These results indicate that *miR-153* disturbs hippocampal synaptic vesicle trafficking by inhibiting synapsin I *in vivo*.

3.4. Knockdown of miR-153 rescues synaptic vesicle trafficking in 2VO rats

Having established the role of *miR-153* on synapsin I *in vitro* and *in vivo*, we went on to elucidate the functional impact of *miR-153* knockdown on 2VO rats. We injected lenti-AMO-153 into the bilateral hippocampal CA1 subfields of 2VO rats (Fig. 5A). As predicted, the application of lenti-AMO-153 significantly inhibited the high expression of *miR-153* in the hippocampus of the 2VO rats compared with that in the rats injected with the lenti-pre-mis-*miR-153* oligonucleotide (Fig. 5B). Moreover, the application of lenti-AMO-153 rescued the decrease of synapsin I expression in the hippocampus of 2VO rats (Fig. 5C). And supplementation of lenti-AMO-*153* in 2VO rats significantly reversed the attenuated DRE phase (Fig. 5D & E). These results indicate that *miR-153* knockdown can ameliorate the CCH-induced impairment of glutamatergic vesicle trafficking.

4. Discussion

CCH is proposed as the preclinical state of cognitive impairment and reported to be related to the impairment of synaptic function (de la Torre, 2004; Duncombe et al., 2017; Yang et al., 2017; Völgyi et al., 2018). However, how this impairment occurs is still unexplored. In the present study, we first reported that CCH developed by 2VO surgery impaired the glutamatergic vesicle trafficking in SC-CA1 of hippocampus, which was controlled by upregulating *miR-153* mediated downregulation of synpasin I. And it is the first to report the molecular mechanism of CCH-mediated impairment of synaptic vesicle trafficking at the microRNA level.

Synaptic vesicles are spatially organized into the three pools: the RRP, recycling pool and reserve pool (Rizzoli and Betz, 2005; Denker and Rizzoli, 2010). Vesicles in the RRP are generally assumed to be both docked and primed at the active zone and likely to fuse with presynaptic membrane in response to a single action potential (Sudhof, 2013a; Zhou et al., 2017). The initial response enhancement of chemical synapses following high-frequency afferent stimulation is presumably derived from vesicles that already present in the RRP (Junge et al., 2004; Schluter et al., 2006; Jensen et al., 2007). While a low-frequency stimulation at 10–20 Hz in excitatory glutamatergic synapses of mouse brain slices was found could induce a delayed response enhancement (DRE), which was considered originating from the vesicle trafficking process from reserve pool or recycling pool to the RRP (Jensen et al., 2007). However, no report about DRE phenomenon was performed in the rats. To observe the synaptic vesicle trafficking in rat hippocampus, we first established the experimental protocol to induce the DRE phenomenon in rat hippocampus referring to previous study in the mouse (Jensen et al., 2007; Hvalby et al., 2010). We found that similar with mouse brain slice, it was 29 °C bath but not the 24 °C bath maintained the suitable reaction of rat brain. Different from mouse hippocampus, it was 10 Hz electric stimulation frequency on rat

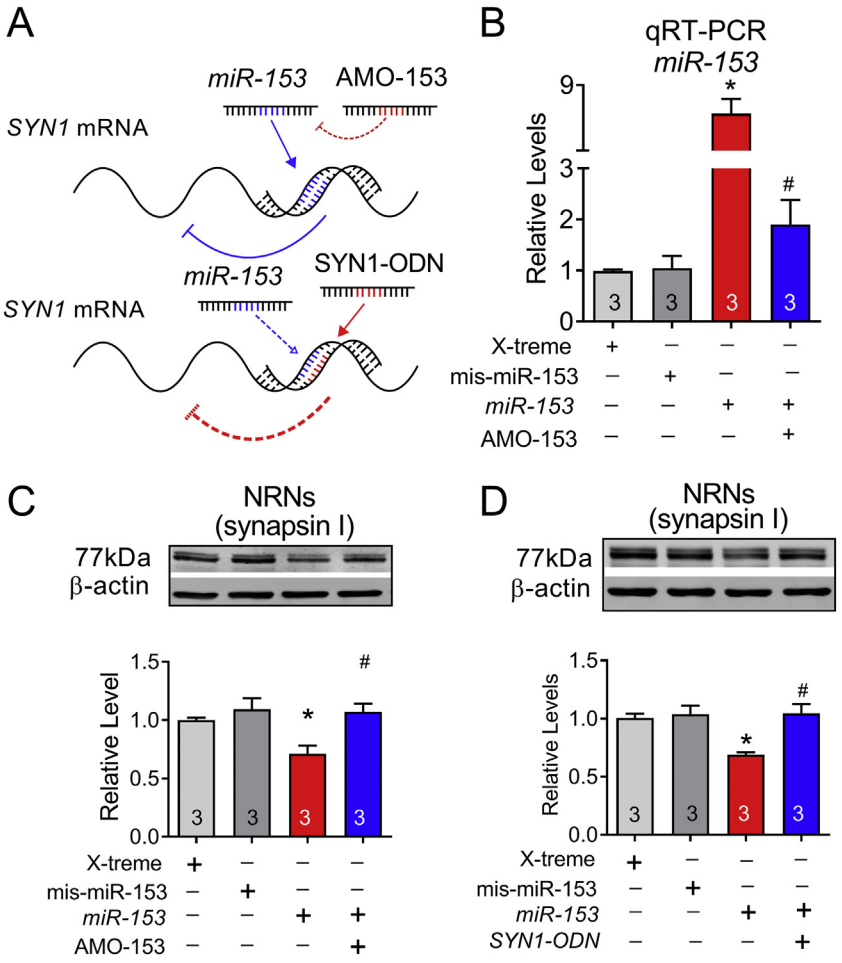

Fig. 3. *MiR-153* inhibits syanpsin I expression with sequence specificity *in vitro*. (A) Schematic diagram of *miR-153* silencing using antisense antagonist and miR-mask technique. Top, *miR-153* binds to complementary target sites in the 3′UTRs of *SYN1* gene, which could be blocked by its antisense antagonist AMO-153. Bottom, Gene-specific ODNs (designed as 22 oligonucleotides fully complementary to the complete sequence of *miR-153* target sites in the 3′UTRs of target mRNAs), which binds with the target sites of *miR-153* in the 3′UTRs of *SYN1* gene to mask the action of *miR-153*. (B) Verification of transfection efficiency of *miR-153* in NRNs after transfection of *miR-153* mimics and AMO-153. (C) *MiR-153* downregulates synapsin I protein levels in primary cultured NRNs compared to *mis-miR-153* transfection. Cells were transfected with *miR-153* mimics, *miR-153* mimics + AMO-153, or mis-*miR-153*. (D) Co-transfection of *SYN1*-ODN with *miR-153* mimics reversed the protein level of synapsin I in NRNs transfected with *miR-153* mimics alone. $n = 3$ batches of cells. $^{*}P < .05$ *vs* mis-*miR-153*; $^{\#}P < .05$ *vs* *miR-153*. Error bars, s. e. m.

hippocampal SC fibers elicited a standard DRE curve which was similar to that in mouse brain slice. When the frequency of electric stimulation was set on 20 Hz, although it can successfully induce DRE in mouse, the DRE curve in rats vanished and was replaced by a continuous decline of fEPSP slope. We speculate that it is due to the trafficking of RP vesicles in rat SC-CA1 synapses need a longer time than that in mice. But the detail mechanism needs to be clarified in the future. Even so, this is the first time to report the experimental parameters for eliciting the DRE curve in rat hippocampal slice. The stimulation frequency of 10 Hz and bath temperature at 29 °C would be the best experimental parameters for the future study on synaptic vesicle trafficking in adult rat hippocampal slices. By using this protocol, we found a significant shortened DRE phase in 2VO rats, indicating an impaired hippocampal glutamatergic vesicle trafficking process.

Maintaining the dynamic equilibrium between the reserve pool and the RRP of vesicles guarantees continued neurotransmitter release from nerve cells (Rizzoli and Betz, 2005). Therefore, the proteins involving the formation and maintenance of the reserve pool and RRP are prime candidates for modulating the efficiency of synaptic transmission (Rosahl et al., 1993; Cesca et al., 2010). It has been demonstrated that vesicles trafficking from the reserve pool to the RRP is regulated by synapsin I/II and its co-factor CaMK II (Benfenati et al., 1992; Torri et al., 1992; Rizzoli and Betz, 2005). Strikingly, consistent with the shortened DRE phase, we found a reduced expression of both synapsin proteins and their phosphorylation in the hippocampus of 2VO rats in the present study. The unchanged CaMK II level suggests that the decreased phospho-synapsin I is the result of decreased synapsin I but not the result of CaMK II deficiency.

MicroRNAs usually have plenty of target genes, and these target genes might play distinct roles in different conditions. For example, several previously studies reported that hypoxia could induce the upregulation of *miR-153* that suppressed tube formation of primary human umbilical vein endothelial cells (HUVECs) and breast cancer angiogenesis by decreasing the secretion of VEGFA *via* targeting the 3′UTR of HIF-1α mRNA (Liang et al., 2018); participated oxygen-glucose deprivation and reoxygenation (OGD/R)-induced injury and oxidative stress in neurons by acting on nuclear factor erythroid 2-related factor 2 (Nrf2) (Ji et al., 2017). However, under severe ischemia at 24 h and 48 h following a permanent middle cerebral artery occlusion, *miR-153* was found decreased that was considered to block angiogenesis by inhibiting HIF-1α (Li et al., 2017). The controversial results may due to the duration or degree of hypoxia. Importantly, Mathew, et al. reported that contextual fear-conditioning by foot shocks induced upregulation of *miR-153* that could impair neurotransmitter release by down-regulating synaptic proteins SNAP25 and VAMP2, as well as glutamate receptor A1, thus influence fear memory formation (Mathew et al., 2016). Our previous study also found that *miR-153* was increased in the hippocampus of rats, and post-transcriptionally inhibited the expression of vesicle release-related proteins by targeting the 3′UTRs of the *Stx1a*, *Snap25*, *Vamp2* and *Syt1* gene following mild cerebral ischemia achieved by 8-week CCH (Yan et al., 2020). In the present study, we found that CCH-induced upregulation of *miR-153* could also targeted the *SYN1* gene and post-transcriptionally inhibited the expression of synapsin I which was proved by using dual-luciferase reporter, antisense siRNA and miRNA-masking techniques based on bioinformatics prediction. Consistent with the regulatory effect of *miR-153* on synapsin I, lenti-pre-*miR-153* elicited a shortened DRE duration similar to that observed in 2VO rats. And these impairments were reversed by the co-injection of lenti-AMO-153. Notably, lenti-AMO-*153* injections significantly prolonged the DRE duration in 2VO rats. These results

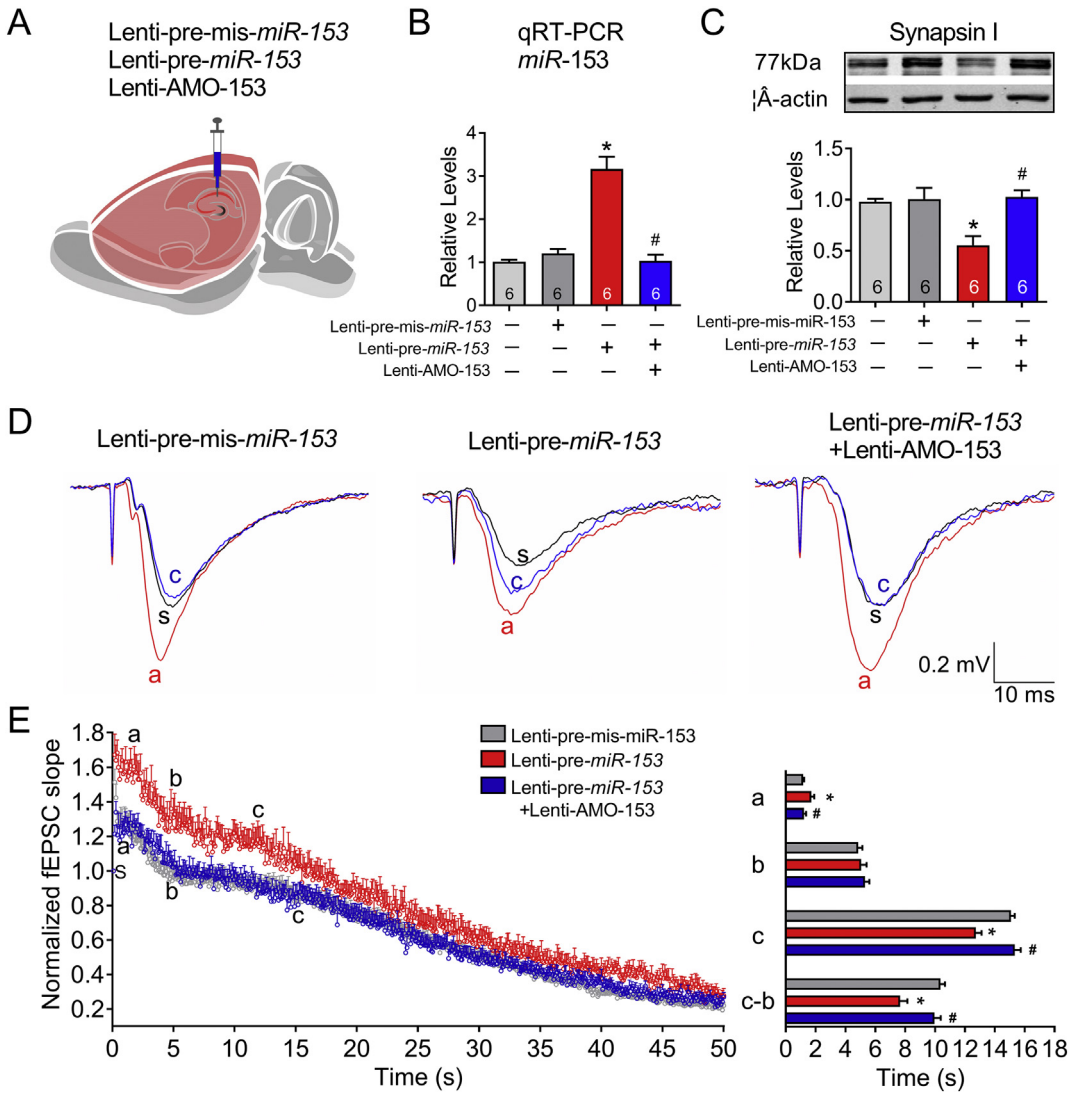

Fig. 4. *MiR-153* impairs hippocampal synaptic vesicle trafficking. (A) Schematic diagram of stereotactic lentivirus injection into CA1 region of hippocampus. (B) Relative levels of *miR-153* in hippocampus of rats injected with lenti-pre-mis-*miR-153*, lenti-pre-*miR-153*, lenti-pre-*miR-153* + lenti-AMO-153. n = 6. $^{*}P < .05$ *vs* Lenti-pre-mis-*miR-153*; $^{\#}P < .05$ *vs* Lenti-pre-*miR-153*. (C) *MiR-153* gain of function by injecting lenti-pre-*miR-153* represses the protein level of synapsin I in hippocampal synaptosomes of rats, which was prevented by lenti- AMO-153. n = 6. $^{*}P < .05$ *vs* Lenti-pre-mis-*miR-153*; $^{\#}P < .05$ *vs* Lenti-pre-*miR-153*. (D) Samples fEPSP traces of lenti-pre-mis-*miR-153*, lenti-pre-*miR-153*, and lenti-pre-*miR-153*+ lenti-AMO-153 treated rats during 10 Hz frequency stimulation. s trace (black), a trace (red), and c trace (blue) reflect the fEPSP at baseline, peak and DRE transition point during 10 Hz stimulation. (E) Left panel is the average traces following 10 Hz frequency stimulation with the increase of recording time in rats SC-CA1 pathway intervention with lenti-pre-mis-*miR-153* (gray, n = 8), lenti-pre-*miR-153* (red, *n* = 9), and lenti-pre-*miR-153*+ lenti-AMO-153 (blue, n = 9). Right panel shows a comparison of the changes with the increase of recording time in point *a*, *b*, *c*, and *c-b* among lenti-pre-mis-miR-153 (gray), lenti-pre-*miR-153* (red), and Lenti-pre-*miR-153* + lenti-AMO-153 (blue) treated rats. $^{*}P < .05$ *vs* Lenti-pre-mis-*miR-153*; $^{\#}P < .05$ *vs* Lenti-pre-*miR-153*. Error bars, s. e. m. (For interpretation of the references to colour in this figure legend, the reader is referred to the web version of this article.)

provided sound evidence that 2VO rats presented disturbed vesicle trafficking, which was controlled by *miR-153* mediated post-transcriptionally repression of synapsin I. Noteworthy, some previous studies have reported that *miR-153* might involve in protective effect on APP/PS1 mice by downregulating the expression of amyloid precursor protein (APP) and amyloid precursor-like protein 2 (APLP2) (Liang et al., 2012); on Parkinson's disease by downregulating α-synuclein (Doxakis, 2010) and on refractory epilepsy by inhibiting HIF-1α (Li et al., 2016). However, these studied just focused on the correlation of expression level between *miR-153* and its targets in the mouse brain (Liang et al., 2012) or patients brain and plasma (Li et al., 2016) as well as the regulatory effect of *miR-153 in vitro* without *in vivo* intervention. Whether *miR-153* could alleviate the pathophysiological process in diseased animal model is an answer worth waiting for. Our recent published work showed that knockdown of *miR-153* could rescue the spatial memory ability of 2VO rats *in vivo* (Yan et al., 2020). Collectively, we get the conclusion that knockdown of *miR-153* may be a potential drug target for alleviating the cognitive impairment involving cerebral ischemia or hypoxemia. While the potential function of *miR-153* in other types of dementia or other nervous system disease needs more evidences.

According to our results, the protein levels of synapsin I and synapsin II were both decreased in 2VO hippocampus. Computational analysis indicates no binding sites between *miR-153* and 3′UTR of *SYN II* gene. However, we found a single subtype (synapsin I) knockdown by lenti-pre-*miR-153* could also impair the glutamatergic vesicle trafficking process. Lenti-AMO-153 also rescued the expression of synapsin I as well as the impairment of hippocampal synaptic vesicle trafficking in 2VO rats in spite of the inadequate function of synapsin II. These data indicate that, at least in rat hippocampal glutamatergic terminals,

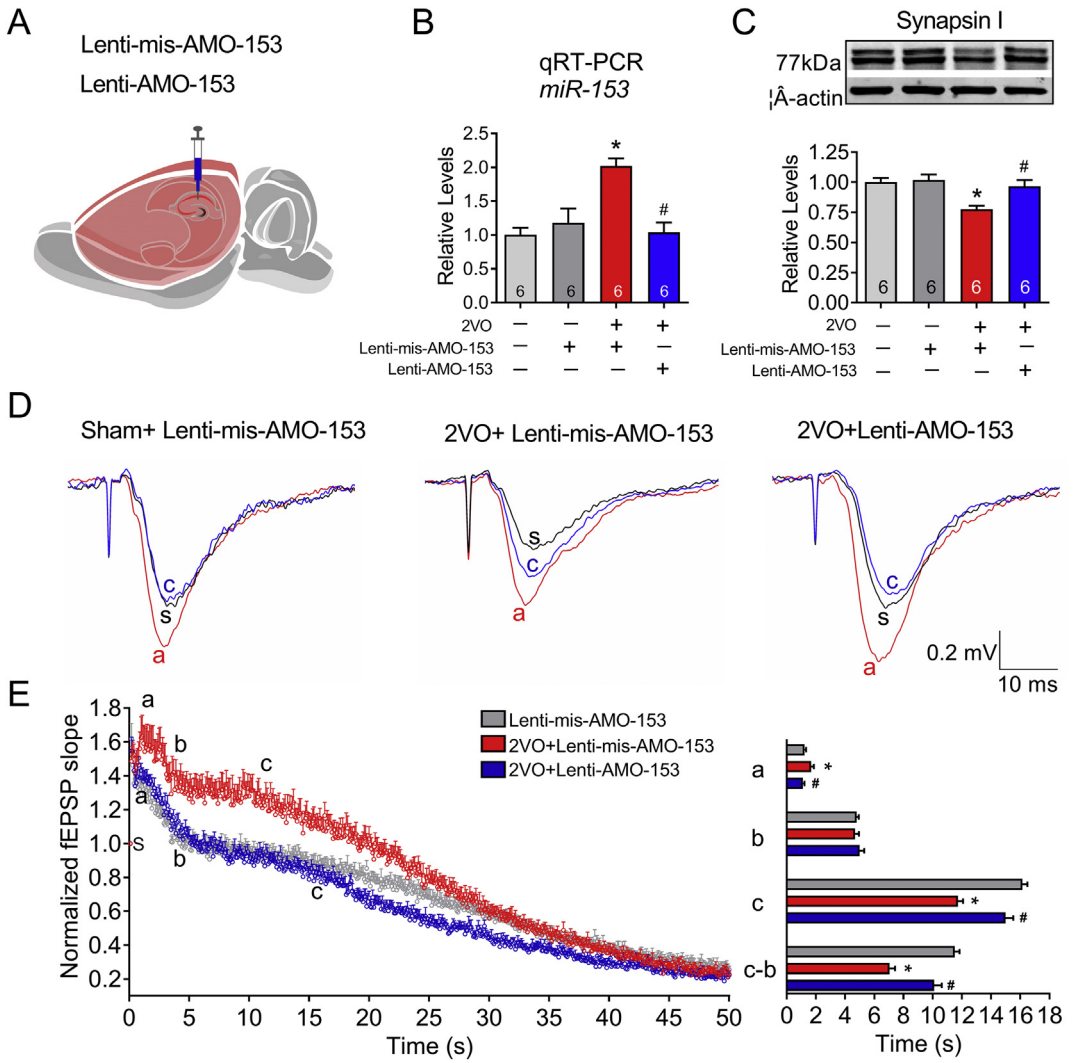

Fig. 5. Knockdown of *miR-153* rescues synaptic vesicle trafficking in 2VO rats. (A) Schematic diagram of stereotactic lentivirus injection into CA1 region of hippocampus. (B) Lenti-AMO-153 injection inhibits *miR-153* expression in hippocampus of 2VO rats. n = 6. $^{*}P < .05$ *vs* Lenti-AMO-*miR-153*; $^{\#}P < .05$ *vs* 2VO + Lenti-mis-AMO-*153*. (C) Knockdown of *miR-153* by injecting lenti-AMO-153 reversed the decreased synapsin I expression induced by 2VO surgery. n = 6. $^{*}P < .05$ *vs* Lenti-AMO-*miR-153*; $^{\#}P < .05$ *vs* 2VO + Lenti-mis-AMO-*153*. (D) Sample fEPSP traces of sham + lenti-pre-mis-miR-153, 2VO + lenti-pre-miR-153, and 2VO + lenti-AMO-153 rats during 10 Hz frequency stimulation. s trace (black), a trace (red), and c trace (blue) reflect the fEPSP at baseline, peak and DRE transition point during 10 Hz stimulation. (E) Knockdown of *miR-153* prevents shortened DRE duration induced by 2VO. Left panel is the average traces following 10 Hz frequency stimulation with the increase of recording time in rats SC-CA1 pathway intervention with sham + lenti-pre-mis-*miR-153* (gray, *n* = 7), 2VO + lenti-pre-*miR-153* (red, n = 8), and 2VO + lenti-AMO-153 (blue, *n* = 10). Right panel shows a comparison of the changes in point *a*, *b*, *c*, and *c-b* among sham + lenti-pre-mis-AMO-153 (gray), 2VO + lenti-mis-AMO-153 (red), and 2VO + lenti-AMO-153 (blue) groups. $^{*}P < .05$ *vs* Lenti-mis-AMO-153; $^{\#}P < .05$ *vs* 2VO + lenti-mis-AMO-153. Error bars, s. e. m. (For interpretation of the references to colour in this figure legend, the reader is referred to the web version of this article.)

synapsin I is more important than synapsin II for synaptic vesicle trafficking (Nichols et al., 1992). Supplementation of synapsin I can compensate for the loss of synapsin II. This working machinery is different from that in mice (Gitler et al., 2008; Song and Augustine, 2015).

Previous study shows that hypoxia stimulated endoplasmic reticulum (ER) stress activates IRE1α and its downstream transcription factor X-box binding protein 1 (XBP1). XBP1 directly binds to the promoter of the *miR-153* host gene *PTPRN* and activates transcription (Liang et al., 2018). CCH, as a chronic hypoxia process, can induce ER stress (Jia et al., 2015). And CCH induced β-amyloid accumulation also triggers ES stress (Ai et al., 2013; Xu et al., 2019). Therefore, we consider CCH induced ER stress as the main reason for *miR-153* upregulation in 2VO rats, which needs to be further verified in future studies.

In summary, we demonstrated that CCH developed by 2VO surgery resulted in impaired hippocampal glutamatergic vesicle trafficking. The disturbed process was controlled by *miR-153*, which post-transcriptionally repressed the expression of vesicle trafficking-related protein synapsin I by targeting the 3′UTRs of the *SYN1* genes. Overexpression of *miR-153* in rat hippocampus could mimic the effects of CCH, while knockdown of hippocampal *miR-153* could rescue the glutamatergic vesicle trafficking *in vivo*. These results will provide important references for drug research and treatment of VaD.

Availability of data and materials

The data used in this study are available from the corresponding author upon reasonable request.

Author contributions

J.A. designed and supervised the study. J.A., S.Z. and M.L.Y. designed the experiments. J.A. and S.Z. wrote the manuscript. S.Z., L.Y. and X.B.A. performed the electrophysiological experiments. M.L.Y., H.M.Z and S.N.X performed the cell culture and PCR experiments.

M.L.Y., S.N.X, J.Z, H.M.Z., S.Y. H., Y. Q., and X.Y. Z. performed the Western blotting. M.L.Y. and S.N.X performed the stereotaxic injections.

Declaration of Competing Interest

The authors declare no conflict of interest.

Acknowledgements

This work was supported by the Natural Science Foundation of China (81870849, 81671052, and 81471115 to J. A.), The Key Project of the Natural Science Foundation of Heilongjiang Province (ZD2018004) to Jing Ai and Heilongjiang Touyan Innovation Team Program.

Appendix A. Supplementary data

Supplementary data to this article can be found online at https://doi.org/10.1016/j.expneurol.2020.113389.

References

Ai, J., Sun, L.H., Che, H., Zhang, R., Zhang, T.Z., Wu, W.C., Su, X.L., Chen, X., Yang, G., Li, K., Wang, N., Ban, T., Bao, Y.N., Guo, F., Niu, H.F., Zhu, Y.L., Zhu, X.Y., Zhao, S.G., Yang, B.F., 2013. MicroRNA-195 protects against dementia induced by chronic brain hypoperfusion via its anti-amyloidogenic effect in rats. J. Neurosci. 33, 3989–4001. https://doi.org/10.1523/JNEUROSCI.1997-12.2013.

Benfenati, F., Valtorta, F., Rubenstein, J.L., Gorelick, F.S., Greengard, P., Czernik, A.J., 1992. Synaptic vesicle-associated Ca2+/calmodulin-dependent protein kinase II is a binding protein for synapsin I. Nature 359, 417–420. https://doi.org/10.1038/359417a0.

Bhuvanendran, S., Bakar, S.N.S., Kumari, Y., Othman, I., Shaikh, M.F., Hassan, Z., 2019. Embelin improves the spatial memory and hippocampal long-term potentiation in a rat model of chronic cerebral hypoperfusion. Sci. Rep. 9, 14507. https://doi.org/10.1038/s41598-019-50954-y.

Bogen, I.L., Jensen, V., Hvalby, O., Walaas, S.I., 2009. Synapsin-dependent development of glutamatergic synaptic vesicles and presynaptic plasticity in postnatal mouse brain. Neuroscience 158, 231–241. https://doi.org/10.1016/j.neuroscience.2008.05.055.

Bogen, I.L., Jensen, V., Hvalby, O., Walaas, S.I., 2011. Glutamatergic neurotransmission in the synapsin I and II double knock-out mouse. Semin. Cell Dev. Biol. 22, 400–407. https://doi.org/10.1016/j.semcdb.2011.07.004.

Bolay, H., Gursoy-Ozdemir, Y., Sara, Y., Onur, R., Can, A., Dalkara, T., 2002. Persistent defect in transmitter release and synapsin phosphorylation in cerebral cortex after transient moderate ischemic injury. Stroke 33, 1369–1375.

Cesca, F., Baldelli, P., Valtorta, F., Benfenati, F., 2010. The synapsins: key actors of synapse function and plasticity. Prog. Neurobiol. 91, 313–348. https://doi.org/10.1016/j.pneurobio.2010.04.006.

Che, H., Yan, Y., Kang, X.H., Guo, F., Yan, M.L., Liu, H.L., Hou, X., Liu, T., Zong, D.K., Sun, L.L., Bao, Y.N., Sun, L.H., Yang, B.F., Ai, J., 2017. MicroRNA-27a promotes inefficient lysosomal clearance in the hippocampi of rats following chronic brain hypoperfusion. Mol. Neurobiol. 54, 2595–2610. https://doi.org/10.1007/s12035-016-9856-8.

Chen, X., Jiang, X.M., Zhao, L.J., Sun, L.L., Yan, M.L., Tian, Y., Zhang, S., Duan, M.J., Zhao, H.M., Li, W.R., Hao, Y.Y., Wang, L.B., Xiong, Q.J., Ai, J., 2017. MicroRNA-195 prevents dendritic degeneration and neuron death in rats following chronic brain hypoperfusion. Cell Death Dis. 8, e2850. https://doi.org/10.1038/cddis.2017.243.

Corradi, A., Zanardi, A., Giacomini, C., Onofri, F., Valtorta, F., Zoli, M., Benfenati, F., 2008. Synapsin-I- and synapsin-II-null mice display an increased age-dependent cognitive impairment. J. Cell Sci. 121, 3042–3051. https://doi.org/10.1242/jcs.035063.

de la Torre, J.C., 2004. Is Alzheimer's disease a neurodegenerative or a vascular disorder? Data, dogma, and dialectics. Lancet Neurol. 3, 184–190. https://doi.org/10.1016/S1474-4422(04)00683-0.

de la Torre, J., 2018. The vascular hypothesis of Alzheimer's disease: a key to preclinical prediction of dementia using neuroimaging. J. Alzheimer's Dis. 63, 35–52. https://doi.org/10.3233/JAD-180004.

Denker, A., Rizzoli, S.O., 2010. ynaptic vesicle pools: an update. Front. Synaptic Neurosci. 2, 135. https://doi.org/10.3389/fnsyn.2010.00135.

Doxakis, E., 2010. Post-transcriptional regulation of alpha-synuclein expression by mir-7 and mir-153. J. Biol. Chem. 285, 12726–12734. https://doi.org/10.1074/jbc.M109.086827.

Duncombe, J., Kitamura, A., Hase, Y., Ihara, M., Kalaria, R.N., Horsburgh, K., 2017. Chronic cerebral hypoperfusion: a key mechanism leading to vascular cognitive impairment and dementia. Closing the translational gap between rodent models and human vascular cognitive impairment and dementia. Clin. Sci. 131, 2451–2468. https://doi.org/10.1042/CS20160727.

Fang, C., Li, Q., Min, G., Liu, M., Cui, J., Sun, J., Li, L., 2017. MicroRNA-181c ameliorates cognitive impairment induced by chronic cerebral Hypoperfusion in rats. Mol. Neurobiol. 54, 8370–8385. https://doi.org/10.1007/s12035-016-0268-6.

Farkas, E., Luiten, P.G., Bari, F., 2007. Permanent, bilateral common carotid artery occlusion in the rat: a model for chronic cerebral hypoperfusion-related neurodegenerative diseases. Brain Res. Rev. 54, 162–180. https://doi.org/10.1016/j.brainresrev.2007.01.003.

Forner, S., Baglietto-Vargas, D., Martini, A.C., Trujillo-Estrada, L., LaFerla, F.M., 2017. Synaptic impairment in Alzheimer's disease: a dysregulated symphony. Trends Neurosci. 40, 347–357. https://doi.org/10.1016/j.tins.2017.04.002.

Gitler, D., Takagishi, Y., Feng, J., Ren, Y., Rodriguiz, R.M., Wetsel, W.C., Greengard, P., Augustine, G.J., 2004. Different presynaptic roles of synapsins at excitatory and inhibitory synapses. J. Neurosci. 24, 11368–11380. https://doi.org/10.1523/JNEUROSCI.3795-04.2004.

Gitler, D., Cheng, Q., Greengard, P., Augustine, G.J., 2008. Synapsin IIa controls the reserve pool of glutamatergic synaptic vesicles. J. Neurosci. 28, 10835–10843. https://doi.org/10.1523/JNEUROSCI.0924-08.2008.

Hackett, J.T., Ueda, T., 2015. Glutamate release. Neurochem. Res. 40, 2443–2460. https://doi.org/10.1007/s11064-015-1622-1.

He, Y., Wei, M., Wu, Y., Qin, H., Li, W., Ma, X., Cheng, J., Ren, J., Shen, Y., Chen, Z., Sun, B., Huang, F.D., Shen, Y., Zhou, Y.D., 2019. Amyloid β oligomers suppress excitatory transmitter release via presynaptic depletion of phosphatidylinositol-4,5-bisphosphate. Nat. Commun. 10, 1193. https://doi.org/10.1038/s41467-019-09114-z.

Ho, L., Guo, Y., Spielman, L., Petrescu, O., Haroutunian, V., Purohit, D., Czernik, A., Yemul, S., Aisen, P.S., Mohs, R., Pasinetti, G.M., 2001. Altered expression of a-type but not b-type synapsin isoform in the brain of patients at high risk for Alzheimer's disease assessed by DNA microarray technique. Neurosci. Lett. 298, 191–194.

Hu, S., Wang, H., Chen, K., Cheng, P., Gao, S., Liu, J., Li, X., Sun, X., 2015. MicroRNA-34c downregulation ameliorates amyloid-beta-induced synaptic failure and memory deficits by targeting VAMP2. J. Alzheimer's Dis. 48, 673–686. https://doi.org/10.3233/JAD-150432.

Hua, S., Wang, B., Chen, R., Zhang, Y., Zhang, Y., Li, T., Dong, L., Fu, X., 2019. Neuroprotective effect of dichloromethane extraction from Piper nigrum L. and Piper longum L. on permanent focal cerebral ischemia injury in rats. J. Stroke Cerebrovasc. Dis. 28, 751–760. https://doi.org/10.1016/j.jstrokecerebrovasdis.2018.11.018.

Hvalby, O., Jensen, V., Kao, H.T., Walaas, S.I., 2010. Synapsin-dependent vesicle recruitment modulated by forskolin, phorbol ester and ca in mouse excitatory hippocampal synapses. Front. Synaptic Neurosci. 2, 152. https://doi.org/10.3389/fnsyn.2010.00152.

Jensen, V., Walaas, S.I., Hilfiker, S., Ruiz, A., Hvalby, O., 2007. A delayed response enhancement during hippocampal presynaptic plasticity in mice. J. Physiol. 583, 129–143. https://doi.org/10.1113/jphysiol.2007.131300.

Ji, Q., Gao, J., Zheng, Y., Liu, X., Zhou, Q., Shi, C., Yao, M., Chen, X., 2017. Inhibition of microRNA-153 protects neurons against ischemia/reperfusion injury in an oxygen-glucose deprivation and reoxygenation cellular model by regulating Nrf2/HO-1 signaling. J. Biochem. Mol. Toxicol. 31. https://doi.org/10.1002/jbt.21905.

Jia, Y., Jin, W., Xiao, Y., Dong, Y., Wang, T., Fan, M., Xu, J., Meng, N., Li, L., Lv, P., 2015. Lipoxin A4 methyl ester alleviates vascular cognition impairment by regulating the expression of proteins related to autophagy and ER stress in the rat hippocampus. Cell. Mol. Biol. Lett. 20, 475–487. https://doi.org/10.1515/cmble-2015-0027.

Junge, H.J., Rhee, J.S., Jahn, O., Varoqueaux, F., Spiess, J., Waxham, M.N., Rosenmund, C., Brose, N., 2004. Calmodulin and Munc13 form a Ca2+ sensor/effector complex that controls short-term synaptic plasticity. Cell 118, 389–401. https://doi.org/10.1016/j.cell.2004.06.029.

Kamat, P.K., Kalani, A., Tyagi, N., 2014. Method and validation of synaptosomal preparation for isolation of synaptic membrane proteins from rat brain. MethodsX 1, 102–107. https://doi.org/10.1016/j.mex.2014.08.002.

Li, Y., Huang, C., Feng, P., Jiang, Y., Wang, W., Zhou, D., Chen, L., 2016. Aberrant expression of miR-153 is associated with overexpression of hypoxia-inducible factor-1α in refractory epilepsy. Sci. Rep. 6, 32091. https://doi.org/10.1038/srep32091.

Li, L., Wang, M., Mei, Z., Cao, W., Yang, Y., Wang, Y., Wen, A., 2017. lncRNAs HIF1A-AS2 facilitates the up-regulation of HIF-1α by sponging to miR-153-3p, whereby promoting angiogenesis in HUVECs in hypoxia. Biomed. Pharmacother. 96, 165–172. https://doi.org/10.1016/j.biopha.2017.09.113.

Liang, C., Zhu, H., Xu, Y., Huang, L., Ma, C., Deng, W., Liu, Y., Qin, C., 2012. MicroRNA-153 negatively regulates the expression of amyloid precursor protein and amyloid precursor-like protein 2. Brain Res. 1455, 103–113. https://doi.org/10.1016/j.brainres.2011.10.051.

Liang, H., Xiao, J., Zhou, Z., Wu, J., Ge, F., Li, Z., Zhang, H., Sun, J., Li, F., Liu, R., Chen, C., 2018. Hypoxia induces miR-153 through the IRE1alpha-XBP1 pathway to fine tune the HIF1alpha/VEGFA axis in breast cancer angiogenesis. Oncogene 37, 1961–1975. https://doi.org/10.1038/s41388-017-0089-8.

Liu, C.D., Wang, Q., Zong, D.K., Pei, S.C., Yan, Y., Yan, M.L., Sun, L.L., Hao, Y.Y., Mao, M., Xing, W.J., Ren, H., Ai, J., 2016. Knockdown of microRNA-195 contributes to protein phosphatase-2A inactivation in rats with chronic brain hypoperfusion. Neurobiol. Aging 45, 76–87. https://doi.org/10.1016/j.neurobiolaging.2016.05.010.

Mannironi, C., Biundo, A., Rajendran, S., De Vito, F., Saba, L., Caioli, S., Zona, C., Ciotti, T., Caristi, S., Perlas, E., Del Vecchio, G., Bozzoni, I., Rinaldi, A., Mele, A., Presutti, C., 2018. miR-135a regulates synaptic transmission and anxiety-like behavior in amygdala. Mol. Neurobiol. 55, 3301–3315. https://doi.org/10.1007/s12035-017-0564-9.

Mathew, R.S., Tatarakis, A., Rudenko, A., Johnson-Venkatesh, E.M., Yang, Y.J., Murphy, E.A., Todd, T.P., Schepers, S.T., Siuti, N., Martorell, A.J., Falls, W.A., Hammack, S.E., Walsh, C.A., Tsai, L.H., Umemori, H., Bouton, M.E., Moazed, D., 2016. A microRNA negative feedback loop downregulates vesicle transport and inhibits fear memory. eLife 5. https://doi.org/10.7554/eLife.22467.

Mathis, D.M., Furman, J.L., Norris, C.M., 2011. Preparation of acute hippocampal slices from rats and transgenic mice for the study of synaptic alterations during aging and

amyloid pathology. J. Visual. Exp. https://doi.org/10.3791/2330.
Nichols, R.A., Chilcote, T.J., Czernik, A.J., Greengard, P., 1992. Synapsin I regulates glutamate release from rat brain synaptosomes. J. Neurochem. 58, 783–785. https://doi.org/10.1111/j.1471-4159.1992.tb09788.x.
Pantoni, L., 2010. Cerebral small vessel disease: from pathogenesis and clinical characteristics to therapeutic challenges. Lancet Neurol. 9, 689–701. https://doi.org/10.1016/S1474-4422(10)70104-6.
Rajmohan, R., Reddy, P.H., 2017. Amyloid-Beta and Phosphorylated tau accumulations cause abnormalities at synapses of Alzheimer's disease neurons. J. Alzheimer's Dis. 57, 975–999. https://doi.org/10.3233/JAD-160612.
Rizzoli, S.O., Betz, W.J., 2005. Synaptic vesicle pools. Nat. Rev. Neurosci. 6, 57–69. https://doi.org/10.1038/nrn1583.
Rosahl, T.W., Geppert, M., Spillane, D., Herz, J., Hammer, R.E., Malenka, R.C., Südhof, T.C., 1993. Short-term synaptic plasticity is altered in mice lacking synapsin I. Cell 75, 661–670. https://doi.org/10.1016/0092-8674(93)90487-b.
Schluter, O.M., Basu, J., Sudhof, T.C., Rosenmund, C., 2006. Rab3 superprimes synaptic vesicles for release: implications for short-term synaptic plasticity. J. Neurosci. 26, 1239–1246. https://doi.org/10.1523/JNEUROSCI.3553-05.2006.
Selkoe, D.J., 2002. Alzheimer's disease is a synaptic failure. Science (New York, N.Y.) 298, 789–791. https://doi.org/10.1126/science.1074069.
Siegert, S., Seo, J., Kwon, E.J., Rudenko, A., Cho, S., Wang, W., Flood, Z., Martorell, A.J., Ericsson, M., Mungenast, A.E., Tsai, L.H., 2015. The schizophrenia risk gene product miR-137 alters presynaptic plasticity. Nat. Neurosci. 18, 1008–1016. https://doi.org/10.1038/nn.4023.
Song, S.H., Augustine, G.J., 2015. Synapsin isoforms and synaptic vesicle trafficking. Mol. Cell 38, 936–940. https://doi.org/10.14348/molcells.2015.0233.
Sudhof, T.C., 2013a. A molecular machine for neurotransmitter release: synaptotagmin and beyond. Nat. Med. 19, 1227–1231. https://doi.org/10.1038/nm.3338.
Sudhof, T.C., 2013b. Neurotransmitter release: the last millisecond in the life of a synaptic vesicle. Neuron 80, 675–690. https://doi.org/10.1016/j.neuron.2013.10.022.
Sun, L.H., Yan, M.L., Hu, X.L., Peng, L.W., Che, H., Bao, Y.N., Guo, F., Liu, T., Chen, X., Zhang, R., Ban, T., Wang, N., Liu, H.L., Hou, X., Ai, J., 2015. MicroRNA-9 induces defective trafficking of Nav1.1 and Nav1.2 by targeting Navbeta2 protein coding region in rat with chronic brain hypoperfusion. Mol. Neurodegener. 10, 36. https://doi.org/10.1186/s13024-015-0032-9.
Torri, Tarelli F., Bossi, M., Fesce, R., Greengard, P., Valtorta, F., 1992. Synapsin I partially dissociates from synaptic vesicles during exocytosis induced by electrical stimulation. Neuron 9, 1143–1153. https://doi.org/10.1016/0896-6273(92)90072-l.
Völgyi, K., Gulyássy, P., Todorov, M., Puska, G., Badics, K., Hlatky, D., Kékesi, K.A., Nyitrai, G., Czurkó, A., Drahos, L., Dobolyi, A., 2018. Chronic cerebral Hypoperfusion induced synaptic proteome changes in the rat cerebral cortex. Mol. Neurobiol. 55, 4253–4266. https://doi.org/10.1007/s12035-017-0641-0.
Xu, S., Di, Z., He, Y., Wang, R., Ma, Y., Sun, R., Li, J., Wang, T., Shen, Y., Fang, S., Feng, L., Shen, Y., 2019. Mesencephalic astrocyte-derived neurotrophic factor (MANF) protects against Aβ toxicity via attenuating Aβ-induced endoplasmic reticulum stress. J. Neuroinflammation 16, 35. https://doi.org/10.1186/s12974-019-1429-0.
Yan, M., Zhang, S., Zhao, H., Xia, S., Jin, Z., Xu, Y., Yang, L., Qu, Y., Huang, S., Duan, M., Mao, M., An, X., Mishra, C., Zhang, X., Sun, L., Ai, J., 2020. MicroRNA-153 impairs presynaptic plasticity by blocking vesicle release following chronic brain hypoperfusion. Cell Commun. Signal. 18, 57. https://doi.org/10.1186/s12964-020-00551-8.
Yang, C., Zhang, X., Gao, J., Wang, M., Yang, Z., 2017. Arginine vasopressin ameliorates spatial learning impairments in chronic cerebral hypoperfusion via V1a receptor and autophagy signaling partially. Transl. Psychiatry 7, e1174. https://doi.org/10.1038/tp.2017.121.
Yao, P.J., Zhu, M., Pyun, E.I., Brooks, A.I., Therianos, S., Meyers, V.E., Coleman, P.D., 2003. Defects in expression of genes related to synaptic vesicle trafficking in frontal cortex of Alzheimer's disease. Neurobiol. Dis. 12, 97–109.
Zhang, X., Huang, X., Fang, C., Li, Q., Cui, J., Sun, J., Li, L., 2017. miR-124 regulates the expression of BACE1 in the Hippocampus under chronic cerebral hypoperfusion. Mol. Neurobiol. 54, 2498–2506. https://doi.org/10.1007/s12035-016-9845-y.
Zhou, Q., Zhou, P., Wang, A.L., Wu, D., Zhao, M., Sudhof, T.C., Brunger, A.T., 2017. The primed SNARE-complexin-synaptotagmin complex for neuronal exocytosis. Nature 548, 420–425. https://doi.org/10.1038/nature23484.